







Article

Exploring Structure-Activity Relationship in Tacrine-Squaramide Derivatives as Potent Cholinesterase Inhibitors

Barbora Svobodova ^{1,2,†}, Eva Mezeiova ^{1,2,3,†}, Vendula Hepnarova ^{1,2} , Martina Hrabínova ^{1,2} ,
Lubica Muckova ^{1,2} , Tereza Kobrlova ¹ , Daniel Jun ^{1,2} , Ondrej Soukup ^{1,2},
María Luisa Jimeno ⁴, José Marco-Contelles ^{3,*} and Jan Korabecny ^{1,2,*} 

¹ Department of Toxicology and Military Pharmacy, Faculty of Military Health Sciences, Trebesska 1575, 500 01 Hradec Kralove, Czech Republic

² Biomedical Research Centre, University Hospital Hradec Kralove, Sokolska 581, 500 05 Hradec Kralove, Czech Republic

³ Laboratory of Medicinal Chemistry, Institute of General Organic Chemistry, Juan de la Cierva 3, 28006-Madrid, Spain

⁴ Centro de Química Orgánica “Lora-Tamayo” (CSIC), C/Juan de la Cierva 3, 28006-Madrid, Spain

* Correspondence: jmarco@iqog.csic.es (J.M.-C.); jan.korabecny@fnhk.cz (J.K.);
Tel.: +34-91-2587554 (J.M.-C.); +420-495-833-447 (J.K.)

† These authors contributed equally to this paper.

Received: 2 August 2019; Accepted: 17 August 2019; Published: 19 August 2019



Abstract: Tacrine was the first drug to be approved for Alzheimer’s disease (AD) treatment, acting as a cholinesterase inhibitor. The neuropathological hallmarks of AD are amyloid-rich senile plaques, neurofibrillary tangles, and neuronal degeneration. The portfolio of currently approved drugs for AD includes acetylcholinesterase inhibitors (AChEIs) and *N*-methyl-*D*-aspartate (NMDA) receptor antagonist. Squaric acid is a versatile structural scaffold capable to be easily transformed into amide-bearing compounds that feature both hydrogen bond donor and acceptor groups with the possibility to create multiple interactions with complementary sites. Considering the relatively simple synthesis approach and other interesting properties (rigidity, aromatic character, H-bond formation) of squaramide motif, we combined this scaffold with different tacrine-based derivatives. In this study, we developed 21 novel dimers amalgamating squaric acid with either tacrine, 6-chlorotacrine or 7-methoxytacrine representing various AChEIs. All new derivatives were evaluated for their anti-cholinesterase activities, cytotoxicity using HepG2 cell line and screened to predict their ability to cross the blood-brain barrier. In this contribution, we also report *in silico* studies of the most potent AChE and BChE inhibitors in the active site of these enzymes.

Keywords: tacrine; bis(7)-tacrine; 6-chlorotacrine; 7-methoxytacrine; squaramides; Alzheimer’s disease; cholinesterases; *in vitro*; *in silico*

1. Introduction

Alzheimer’s disease (AD), the most common form of dementia [1], is symptomatically treated with inhibitors of acetylcholinesterase (AChE, 3.1.1.7). This type of serine protease catalyzes the hydrolysis of the neurotransmitter acetylcholine (ACh) to choline and acetic acid [2]. Low levels of ACh lead to cognitive impairment and dementia [3], thus the inactivation of AChE increases the pool of ACh and ameliorates the cognitive dysfunction associated with AD [4]. Three AChE inhibitors (AChEIs), namely, donepezil, galantamine, and rivastigmine, are the representatives of so-called “cholinergic hypothesis” used currently as the main drugs for AD treatment [5]. The etiology of AD is complex,

and several factors are considered as causative. Indeed, AD has been recognized by deposition of two types of proteins, extracellularly accumulated β -amyloid ($A\beta$) protein due to abnormal processing of amyloid precursor protein (APP), and intracellular neurofibrillary tangles composed from hyperphosphorylated tau protein [6]. Furthermore, various other neurochemical abnormalities contribute to the progression of AD, such as oxidative stress [7], excitotoxicity [8], imbalance of biometals [9], or neuro-inflammation [10]. Memantine, an antagonist of *N*-methyl-D-aspartate (NMDA) receptor, is also approved for AD treatment [11].

Tacrine (THA, 9-amino-1,2,3,4-tetrahydroacridine, Figure 1) is the centrally acting reversible AChEI that launched the market in 1993 as the first drug to alleviate symptoms of AD [12]. THA is a non-selective cholinesterase agent, inhibiting also butyrylcholinesterase (BChE, E.C. 3.1.1.8). Moreover, it affects several other biological systems, which contributes to its complex action against AD [13]. THA has been reported to also modulate muscarinic and nicotinic receptors [14] and the amyloidogenic pathway [15,16]. The clinical benefits of THA were limited by its poor oral bioavailability and considerable side effects mainly defined as hepatotoxicity. This fact caused THA withdrawal from the market [17,18]. On the other hand, 1,2,3,4-tetrahydroaminoacridine scaffold still stands at the forefront of the scientific research given by its relatively simple structure that can be easily modified to find novel, more potent, and less toxic analogues. Indeed, these endeavors yielded, for instance, 7-methoxytacrine (7-MEOTA) [14], 6-chlorotacrine (6-Cl-THA) [19], or homodimer bis(7)-tacrine [20] (Figure 1). 7-MEOTA possesses suppressed toxicity profile compared to THA due to distinct metabolic pathway preserving anti-ChE potency [14]. The chlorine atom at position 6- of the THA core strongly enhances the inhibitory activity against AChE. 6-Cl-THA has two orders of magnitude higher AChE inhibition potency than THA [21]. Bis-tacrine homodimers were developed as multifunctional analogues capable to simultaneously contact both the catalytic site (CAS) and the peripheral anionic site (PAS) of AChE [20,22]. The most active derivative is connected via seven methylene units (bis(7)-tacrine), being almost 400-fold more potent than THA in inhibiting human AChE [23].

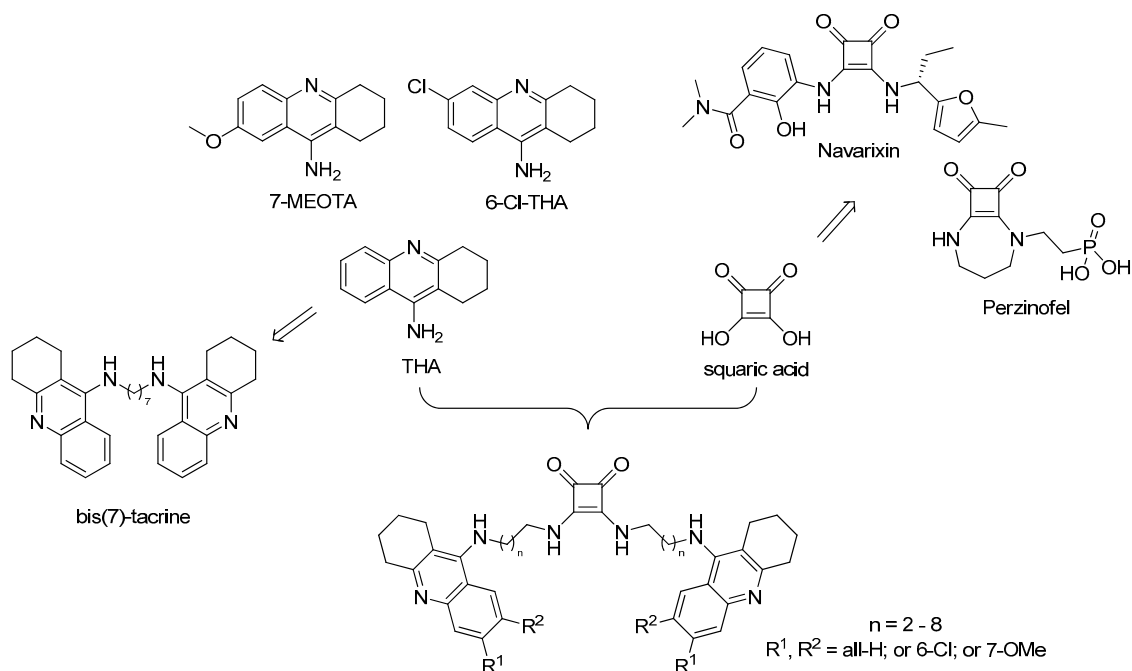


Figure 1. Schematic drawing for the design of tacrine-squaramide homodimers.

Squaramides (SQ) are derivatives of squaric acid (3,4-dihydroxycyclobut-3-ene-1,2-dione) that are widely used in a variety of fields of expertise (Figure 1). They mostly dominate asymmetric synthesis as chiral ligands and H-bonding catalysts [24–27], but are also valuable building blocks in medicinal chemistry. Examples of small molecules with incorporated squaramide scaffold, that reached the various stages of clinical trials, are Perzinfotel (NMDA receptor antagonist) [28], and Navarixin

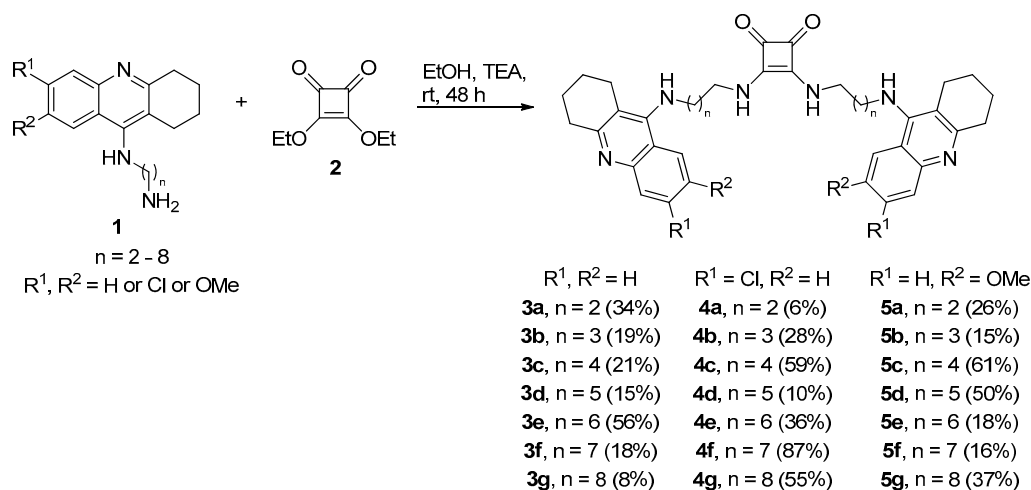
(chemokine receptors 1 and 2 antagonist) [29] (Figure 1). Squaramide can be considered as a motif of interest enabling formation of H-bonds bioisosteric to functionalities like carboxylic and amino acids, urea, guanidine, cyanoguanidine, and different phosphate groups [30]. More recently, mono- and bis-squaramide-based derivatives were investigated as treatment for insect-transmitted parasite diseases such as leishmaniasis [31], malaria [32], and Chagas disease [33].

Considering the simple synthesis and other properties (aromaticity, rigidity, H-bond formation) suitable for binding of squaramide motif, we envisaged to combine this scaffold with different tacrine-based derivatives following the successful story of bis(7)-tacrine. Bis(7)-tacrine has a broad and complex pharmacological profile. Besides highly selective inhibition potency towards AChE, it emerged as a potent inhibitor of other enzymes like β -secretase 1 (BACE-1), nitric-oxide synthase and receptors including NMDA, serotonin 5-HT₃, gamma-aminobutyric acid GABA_A, nicotinic and others, all of them being involved in the pathophysiology of neurodegenerative disorders [23,34–36]. Bis(7)-tacrine is able to inhibit self-aggregation and also AChE-induced aggregation of A β protein [37]. Moreover, bis(7)-tacrine has been shown to provide multiple neuroprotective effects in vitro and in vivo [38–44]. Bis(7)-tacrine has spurred the development of so-called multi-target directed ligands (MTDLs) targeting several pathological mechanisms pathways in AD. In this study, we developed 21 novel dimers amalgamating squaric acid scaffold with THA, 6-Cl-THA, and 7-MEOTA into so-called tacrine-squaramide homodimers (Figure 1). All new derivatives were evaluated for their anti-ChEs properties, cytotoxicity using the HepG2 cell line, and selected compounds were screened to predict their ability to cross the blood-brain barrier (BBB). In this article, we also report in silico studies of the most potent AChE and BChE inhibitors in the active site of respective enzyme.

2. Results and Discussion

2.1. Chemistry

Symmetrical squaramides are generally prepared by the reaction of dialkyloxysquarate derivatives with an excess of primary or secondary amines [30]. Aliphatic amine condensation of corresponding tacrine derivatives **1** with diethoxysquarate (**2**) in ethanol in the presence of TEA afforded desired products with 6–87% yields (THA family—**3a–3g**; 6-Cl-THA family—**4a–4g** and 7-MEOTA family—**5a–5g**; Scheme 1). Intermediates of general structure **1** varying in the length of alkyl chains were prepared according to previously published methods [45,46]. During the synthesis, we also observed the formation of monomeric analogues of squaramides (not shown in the Scheme 1), but these were chemically unstable when isolated and thus were excluded from further biological studies. All final compounds were characterized by ¹H, ¹³C-NMR spectra and HRMS analysis. LC analysis confirmed their purity >95%.



Scheme 1. Synthetic procedure for tacrine-squaramide derivatives **3a–3g**, **4a–4g** and **5a–5g**.

2.2. Evaluation of Cholinesterase Inhibitory Activity

Three series of tacrine-squaramide homodimers were tested for their inhibitory potential against human AChE (*hAChE*) and human BChE (*hBChE*) enzymes using modified spectrophotometric method of Ellman et al. [47–50]. THA, 6-Cl-THA and 7-MEOTA were used as reference compounds. The IC_{50} values of all tested compounds and their selectivity index (SI) for *hAChE* are summarized in Table 1. All tested derivatives showed good to excellent inhibitory potencies for both cholinesterases with IC_{50} values ranging from micromolar to the single digit nanomolar scale.

All homodimers bearing THA (**3a–g**) and 6-Cl-THA (**4a–g**) units displayed IC_{50} values in the nanomolar range for *hAChE* (2–72 nM). As expected, derivatives of 7-MEOTA (**5a–g**) were less potent, displaying IC_{50} values in the sub-micromolar to micromolar range (0.1–4.5 μ M). According to *hAChE* inhibition potency, the top ranked derivative from all the derivatives under the study was **4b** (IC_{50} = 2.0 nM) being only 2.5-times less active compared to bis(7)-tacrine (IC_{50} = 0.8 nM) [51], but still one order of magnitude more potent *hAChEI* than the parent 6-Cl-THA. From THA and 7-MEOTA families, the most pronounced derivatives in terms of *hAChE* inhibition were **3a** and **5d** with IC_{50} values 3.8 and 120 nM, being 84- and 83-times more potent than references THA and 7-MEOTA, respectively. The length of the spacer between two tacrine sub-units significantly affected AChE inhibition potency. THA- and 6-Cl-THA-based dimers (compounds **3f**, **3g**, and **4f**, **4g**) with the longest chains were the least active AChEIs. Surprisingly, for the 7-MEOTA-dimers, negligible inhibitory potency was associated with derivatives bearing shorter linkers, especially to **5b** and **5c**.

Almost all homodimers were also good inhibitors of *hBChE* with IC_{50} values in the micromolar to nanomolar range. The most active *hBChE*Is were THA-based derivatives (IC_{50} = 21–75 nM) followed by 6-Cl-THA and 7-MEOTA subsets. THA-derivative **3e** exerted the highest *hBChE* inhibition potency (IC_{50} = 21 nM).

The selective/non-selective inhibition profile for ChEs in drugs potentially useful in AD treatment is largely discussed [52]. Currently used ChEIs are AChE-selective (donepezil) or possess more or less non-selective pattern of inhibition (rivastigmine, galantamine). It has been proved that levels of BChE in the brain of AD patients are elevated with age while levels of AChE are decreased. This finding underlies the importance of selective-BChEIs in the treatment of moderate-to-severe stages of AD [53]. Given this fact, only **3g** revealed small preference for *hBChE* inhibition (SI = 0.7), while most of the tacrine-squaramides were AChE-selective, highlighting **4g** from the 6-Cl-THA family with remarkable SI > 10,000. In the THA-based subset, SI strongly correlated with the length of alkyl chain where the four-methylene tethered analogue (**3c**) displayed the most pronounced AChE selectivity.

2.3. Kinetic Study of AChE and BChE Inhibition

Kinetic study was performed in order to describe the interactions of the compounds **4b** and **3e** with *hAChE* and *hBChE*, respectively. Inhibition kinetics were elucidated from velocity curves that were measured at several concentrations of the corresponding substrate (AChE—acetylthiocholine, BChE—butyrylthiocholine) and tested compounds. The type of enzyme inhibition and corresponding kinetic parameters (K_i and K_i') were determined by nonlinear regression analysis. Results for each type model of inhibition (competitive, non-competitive, uncompetitive and mixed) were compared by sum-of-squares *F*-test. Statistical analysis showed mixed type of inhibition ($p < 0.05$), which is in line with the Lineweaver–Burk plot, used for visualization of obtained data (Figure 2).

The intersection of lines is located above the *x*-axis for both measured inhibitors, which means reversible binding mode to both free enzyme and enzyme-substrate complex, with higher affinity to the free enzyme ($K_i < K_i'$), interacting with its allosteric peripheral anionic site (PAS). This interaction causes conformational changes of the cholinesterase, resulting also in changes of its active site. K_m was slightly increased and V_{max} was reduced at higher concentration of both inhibitors. A K_i value of 0.4 ± 0.2 nM and K_i' of 0.5 ± 0.2 nM were measured for **4b** on AChE and a K_i value of 8.1 ± 1.9 nM and K_i' of 100 ± 28 nM for **3e** on BChE, respectively.

Table 1. *hAChE* and *hBChE* inhibitory activities of tacrine-squaramide homodimers and reference compounds THA, 6-Cl-THA and 7-MEOTA.

Compound	R ¹	R ²	n	IC ₅₀ (nM) ^a		SI ^b
				<i>hAChE</i>	<i>hBChE</i>	
3a	H	H	2	3.8	62	16
3b	H	H	3	8.4	55	6.5
3c	H	H	4	5.5	75	14
3d	H	H	5	8.1	69	8.5
3e	H	H	6	13	21	1.6
3f	H	H	7	32	32	1
3g	H	H	8	72	50	0.7
4a	Cl	H	2	4.2	150	36
4b	Cl	H	3	2.0	110	55
4c	Cl	H	4	4.6	170	37
4d	Cl	H	5	8.2	310	38
4e	Cl	H	6	3.2	540	170
4f	Cl	H	7	16	450	28
4g	Cl	H	8	10	>100,000	>10,000
5a	H	OMe	2	170	130	0.7
5b	H	OMe	3	1100	8900	8.1
5c	H	OMe	4	4500	4700	0.9
5d	H	OMe	5	120	680	5.7
5e	H	OMe	6	150	1100	7.3
5f	H	OMe	7	170	1300	7.6
5g	H	OMe	8	490	2900	5.9
THA ^c	H	H	-	320	80	0.3
6-Cl-THA ^c	Cl	H	-	20	1800	90
7-MEOTA ^c	H	OMe	-	10,000	17,000	1.7

^a Results are expressed as the mean of at least three experiments; ^b SI = selectivity index, selectivity for *hAChE* is determined as ratio IC₅₀(*hBChE*)/IC₅₀(*hAChE*); ^c data taken from Ref. [45,46,54,55].

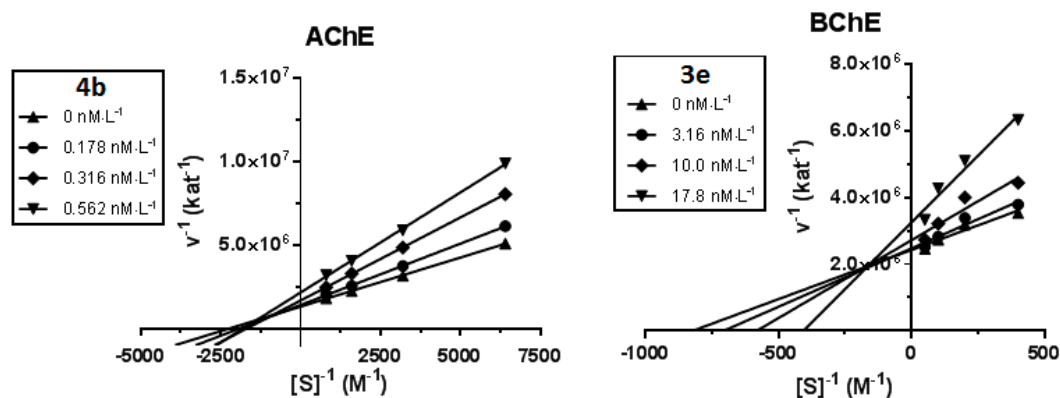


Figure 2. Steady state inhibition of cholinesterase substrate hydrolysis by compound **4b** (*hAChE*) and **3e** (*hBChE*) at different concentrations. Lineweaver–Burk plots of initial velocity at increasing substrate concentrations (*AChE*: 0.1563–1.250 mM; *BChE*: 2.5–20.0 mM) are presented. Lines were derived from a linear regression of the data points.

2.4. Cytotoxicity

The MTT (3-(4,5-dimethylthiazol-2-yl)-2,5-diphenyltetrazolium bromide) colorimetric assay performed on the human hepatocyte carcinoma (HepG2) cell line was applied to investigate the preliminary toxicity profile of all the developed derivatives [56]. The results are summarized in Table 2. The lowest cytotoxic effect displayed analogues with the shortest alkyl chains from all three series (**3a**, **4a**, and **5a**). These compounds were nontoxic at the highest tested concentrations (256 μ M for

3a and **5a**, and 128 μM for **4a**). The linker elongation negatively affected cytotoxicity in THA- and 7-MEOTA-squaramides. In other words, the most toxic hybrids were those having the longest spacers, i.e., compounds **3g** and **5g**, with IC_{50} values 6.6 and 3.5 μM , respectively. Derivatives of 6-Cl-THA were nontoxic even at the highest tested concentration of 64 μM and, intriguingly, were also less toxic than reference 6-Cl-THA ($\text{IC}_{50} = 43 \mu\text{M}$). These data have to be considered carefully since MTT cytotoxicity screening is performed on isolated cell lines, thus these results provide only preliminary toxicity insight and do not reflect the toxicity profile under in vivo conditions. For comparative purposes, we also included cytotoxicity data for other AChEIs like donepezil, galantamine and rivastigmine. Interestingly, donepezil toxicity lies in the same range as some of the least toxic tacrine-squaramides (**3c**, **4a** and **5c**), whereas rivastigmine and galantamine exerted a one to three orders lower toxic profile.

Table 2. Cytotoxicity of tacrine-squaramides evaluated using HepG2 cells measured by colorimetric MTT assay.

Compound	R ¹	R ²	n	IC ₅₀ (μM) ^a
3a	H	H	2	>256
3b	H	H	3	>32
3c	H	H	4	150
3d	H	H	5	69
3e	H	H	6	76
3f	H	H	7	23
3g	H	H	8	6.6
4a	Cl	H	2	>128
4b	Cl	H	3	>64
4c	Cl	H	4	>64
4d	Cl	H	5	>64
4e	Cl	H	6	>64
4f	Cl	H	7	>64
4g	Cl	H	8	>64
5a	H	OMe	2	>256
5b	H	OMe	3	>64
5c	H	OMe	4	190
5d	H	OMe	5	98
5e	H	OMe	6	26
5f	H	OMe	7	9
5g	H	OMe	8	3.5
THA	H	H	-	169
6-Cl-THA	Cl	H	-	43
7-MEOTA	H	OMe	-	44
Donepezil	-	-	-	150
Rivastigmine	-	-	-	3400
Galantamine	-	-	-	4200

^a The IC_{50} values are expressed as the mean of at least three independent experiments.

2.5. In Vitro BBB Permeation

An important feature for drugs targeting the brain is their ability to cross the BBB. The parallel artificial membrane permeability assay (PAMPA) is a high-throughput screening tool applicable for prediction of passive transport across BBB [57]. The results of selected homodimers and positive (THA, donepezil, ibuprofen) and negative (furosemide, chlorothiazide, ranitidine) controls are outlined in Table 3. The studied compound **4e** is likely endowed with a high probability to cross the BBB. Derivatives **3a** and **5d** with lower values of P_e cannot presumably cross the BBB; other tested derivatives have uncertain BBB permeation (**3e**, **4b**, and **5a**). It also has to be bear in mind, that in its current form using lipid porcine, the PAMPA-BBB assay possesses several limitations. These include mainly (i) the different composition of the human phospholipid bilayer may cause deviation in predicted

permeability, (ii) omitting the absorption of compounds that are actively transported by influx transporters and pumped-out by various efflux mechanisms with the glycoprotein P at the forefront or (iii) transport through the paracellular route which is mostly exploited by small hydrophobic molecules [58]. Even considering these drawbacks, PAMPA-BBB is conceived as very simple but powerful tool for BBB prediction.

Table 3. Prediction of BBB penetration of the studied compounds expressed as *Pe* values.

Compound	R ¹	R ²	n	<i>Pe</i> (× 10 ^{−6} cm.s ^{−1}) ^a	CNS (+/−) ^b
3a	H	H	3	1.1	CNS −
3e	H	H	3	2.6	CNS +/-
4b	Cl	H	3	2.5	CNS +/-
4e	Cl	H	6	17.0	CNS +
5a	H	OMe	2	2.3	CNS +/-
5d	H	OMe	5	1.3	CNS −
THA	H	H	-	6.0	CNS +
donepezil				21.0	CNS +
ibuprofen				12.0	CNS +
furosemide				0.0	CNS −
chlorothiazide				0.3	CNS −
ranitidine				0.0	CNS −

^a Results are expressed as the mean of at least three experiments; ^b CNS +: high BBB permeation predicted with *Pe* (10^{−6} cm.s^{−1}) > 4.0, CNS −: low BBB permeation predicted with *Pe* (10^{−6} cm.s^{−1}) < 2.0, CNS +/-: BBB permeation uncertain with *Pe* (10^{−6} cm.s^{−1}) from 4.0 to 2.0.

2.6. In Silico Studies

Molecular docking studies were carried out with the *hAChE* and *hBChE* enzymes to analyze the binding data of the developed compounds. We employed the crystal structures of *hAChE* (PDB entry: 4EY7) bound to dual anionic site ligand donepezil and *hBChE* (PDB entry: 4BDS) complexed with THA [59,60]. Both of them possess satisfactory resolution at 2.35 Å and 2.10 Å, respectively, ensuring reliable outputs. In line with the results from in vitro and following enzyme kinetic analysis, we selected **4b** and **3e**, two most pronounced *hAChE* and *hBChE* inhibitors from 6-Cl-THA and THA families, respectively. Docking analyses were carried out using Autodock Vina software (v. 1.1.2) [61].

Tacrine-squaramide derivative **4b** spans the cavity gorge of *hAChE* from the bottom to the entrance (Figure 3A,B). Proximal 6-Cl-THA unit occupies CAS region by showing typical parallel π - π /cation- π interaction with Trp86 (3.9 Å; distance measured from center-to-center of aromatic rings). Chlorine atom is directed towards hydrophobic groove of the enzyme contacting Tyr124, Ser125 and Asn87. This topology orientation of 6-Cl-THA moiety has been observed more valuable in improving the inhibition potency compared to 7-MEOTA derivatives. The latter generally displays unfavorable 180° rotation of core tacrine scaffold yielding lower enzyme affinity [14,62]. Catalytic triad residues (Glu202, Ser203 and His447) are also involved in ligand stabilization revealing alkyl- π (His447) or van der Waals contacts (Glu202 and Ser203). Connecting linker is anchored via a complex web of hydrophobic interactions in the mid-gorge enzyme region. These also involve distorted π - π contacts between central squaramide scaffold with Tyr341 (4.5 Å), Tyr124 (4.5 Å), Phe297 (4.2 Å) and Phe338 (5.1 Å). The most strikingly aromatic character of squaramide and its interaction with aromatic residues in the mid-gorge region can be denoted as culprits for extraordinary inhibition potency of **4b**. At the rim of the gorge, the distal 6-Cl-THA subunit faces towards key amino acid residue from PAS region, i.e., Trp286 (parallel π - π stacking, 3.7 Å). In general, **4b**-*hAChE* complex mimics structural features in crystallographically refined bis(7)-tacrine in *Torpedo californica* AChE [63].

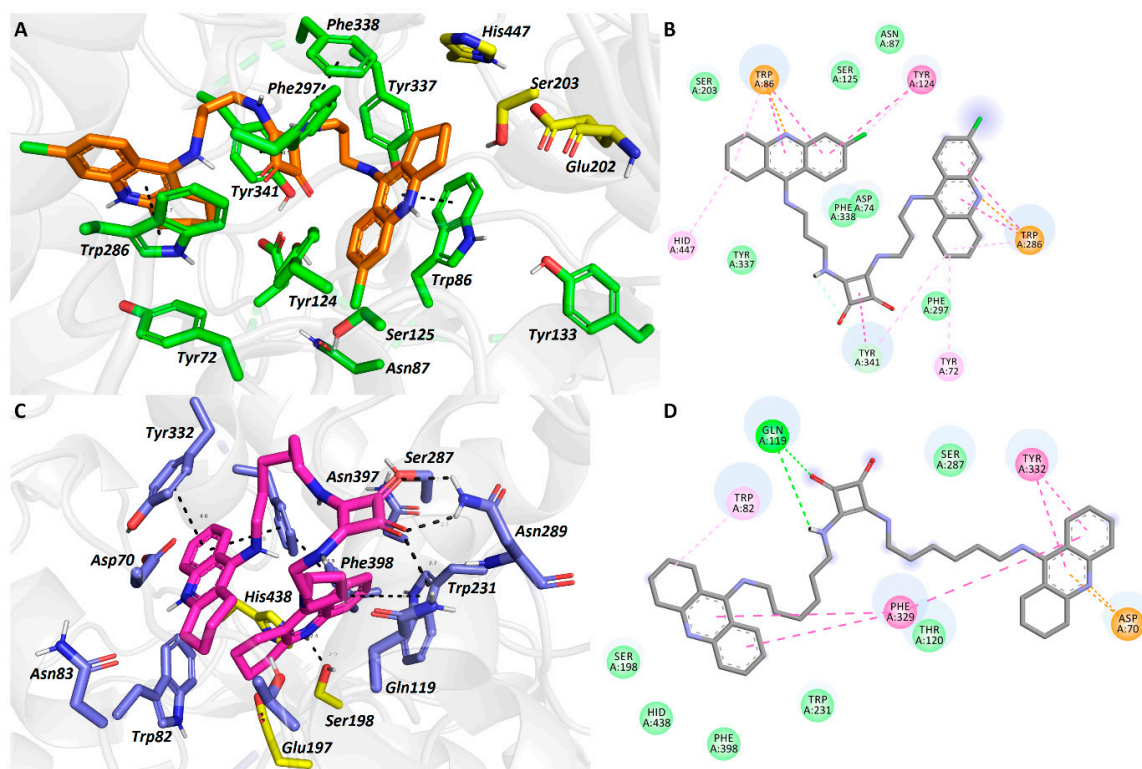


Figure 3. Docking results for the tacrine-squaramide hybrids **4b** and **3e** within *hAChE* (A,B) and *hBChE* (C,D) active sites, respectively (PDB IDs: 4EY7, 4BDS). A and C—Superimposed analogues **4b** and **3e** (orange and purple carbon atoms, respectively) as 3D figures; B and D—2D figures **4b** and **3e**, respectively. Generally to A and C—important amino acid residues involved in the ligand-enzyme interactions are displayed as green and blue carbon atoms, respectively; catalytic triad residues are shown in yellow, the rest of the enzyme is represented as a light-grey cartoon. Figures A and C were generated with PyMol 1.5.0.4 (The PyMOL Molecular Graphics System, Version 1.5.0.4 Schrödinger, LLC, Mannheim, Germany), Figures B and D were created with Discovery Studio 2016 Client software.

In the **3e**-*hBChE* complex, the ligand revealed atypical U-shaped conformation (Figure 3C,D). This can be nicely explained by the structural differences between AChE/BChE enzymes in the PAS region, where most of the aromatic amino acid residues in BChE are substituted by aliphatic ones enabling entrance of more bulky substrates [64]. From this point of view, the structural properties of BChE enabled lodging of both THA subunits of **3e** deep into cavity of *hBChE*. In this case, catalytic triad residues form either hydrophobic (His438 and Glu197) or hydrogen-bond contacts (2.5 Å). The ligand orientation is mainly orchestrated by Phe329 stabilizing both tacrine-subunits and allow ligand U-shaped conformation. Interestingly, the squaramide moiety exerted a complex web of hydrogen bonds with Asn289 (2.3 and 2.3 Å) and Gln119 (2.7 Å) at the mouth of the enzyme.

3. Conclusions

The never-ending quest to find effective therapy for AD is on one hand a challenging task and on the other hand, a daunting process. Enormous efforts are made to find disease-modifying agents that would improve quality of life for the AD sufferers. A wealth of scientific studies currently still indicate that ChEIs can serve as a useful tool in drug development of potential therapeutics to tackle symptomatology of AD as well their beneficial effects on pathophysiological pathways associated with the progression of the disease. Building on them, so-called MTDLs flourished as an emerging direction [65,66]. These findings, given by the drug evolution, can renew the interest in ChEIs but only if rationally designed [67]. In this study, we described the design, synthesis, and in vitro evaluation of squaramide-containing tacrine homodimers represented by THA, 6-CI-THA, and 7-MEOTA scaffolds.

All newly developed compounds were good to excellent inhibitors of both ChEs, with IC_{50} in the micromolar to single-digit nanomolar range. Compounds **4b** and **3e** were found to demonstrate the highest inhibition potencies against *hAChE* and *hBChE*, respectively. For **4b** and **3e**, the kinetic analysis revealed their mixed-type inhibition which is indicative of concurrent interaction with both anionic sites of the enzymes. The lowest cytotoxic effect on HepG2 cell line displayed analogues with the shortest alkyl chains from all three series (**3a**, **4a**, and **5a**). Increasing the number of methylene units in the linker increases the cytotoxicity. Interestingly, this finding does not apply to the 6-Cl-THA family. However, from the six selected squaramide-tacrine homodimers, only **4e** is predicted to be BBB permeable. In silico studies predicted orientation of **4b** in *hAChE* active site correlating well with previously published crystallographic structure of bis(7)-tacrine in AChE. Compound **3e** displayed rather atypical U-shaped conformation in the *hBChE* active site, given presumably by the topological properties of cholinesterase. With this in mind, we believe that squaramides can be further recognized as interesting building blocks in the drug discovery with particular emphasis on AD.

4. Experimental Section

4.1. General Chemistry Methods

All chemical solvents and reagents were used in the highest available purity without further purification and they were purchased from Sigma-Aldrich (Prague, Czech Republic). The reactions were monitored by thin layer chromatography (TLC) on silica gel plates (60 F254, Merck, Prague, Czech Republic) and the spots were visualized by ultraviolet light (254 nm). Purification of crude products was carried out using columns of silica gel (silica gel 100, 0.063–0.200 mm, 70–230 mesh ASTM, Fluka, Prague, Czech Republic). NMR spectra were recorded in deuterated chloroform ($CDCl_3$), deuterated methanol (CD_3OD) and deuterated dimethyl sulfoxide ($DMSO-d_6$) on a Varian S500 spectrometer. Chemical shifts (δ) are reported in parts per millions (ppm) and spin multiplicities are given as bold singlet (bs), doublet (d), doublet of doublet (dd), triplet (t), quartet (q), pentet (p), or multiplet (m). Coupling constants (J) are reported in Hz. Recorded NMR data are available at Supplementary Information. The synthesized compounds were analyzed by an LC-MS system consisting of UHPLC Dionex Ultimate 3000 couplet with Q Exactive Plus mass spectrometer to obtain high resolution mass spectra (Thermo Fisher Scientific, Bremen, Germany). Melting points were measured using an automated melting point recorder M-565 (Büchi, Switzerland). The final compounds were analyzed by LC-MS consisting of UHPLC Dionex Ultimate 3000 RS coupled with Q Exactive Plus orbitrap mass spectrometer (Thermo Fisher Scientific, Bremen, Germany) to obtain high-resolution mass spectra. Gradient LC analysis confirmed > 95% purity.

General Procedure for the Preparation of Tacrine-Squaramides (**3a–3g**; **4a–4g** and **5a–5g**)

To the solution of diethoxysquarate **2** (1.0 eq) in EtOH (1 M) were added corresponding tacrine derivative (2.0 eq) and TEA (2.0 eq). The reaction mixture was stirred at room temperature for 48 h. After completion of the reaction, the solvent was evaporated and crude product was purified by column chromatography using a mixture of eluents (DCM:MeOH:NH₃ = 20:1:0.1).

Bis[(2-[(1,2,3,4-tetrahydroacridin-9-yl)amino]ethyl)amino]cyclobut-3-ene-1,2-dione (**3a**). Yield 34%; yellow solid; M_p = 159–160 °C; ¹H-NMR (500 MHz, CD_3OD): δ 8.06–7.99 (m, 2H), 7.74–7.69 (m, 2H), 7.54–7.47 (m, 2H), 7.36–7.28 (m, 2H), 3.79–3.60 (m, 8H), 2.95–2.88 (m, 4H), 2.72–2.61 (m, 4H), 1.88–1.75 (m, 8H); ¹³C-NMR (126 MHz, CD_3OD): δ 183.6 (CO), 158.7, 153.2, 146.8, 137.8, 130.3, 127.2, 125.3, 124.2, 121.1, 117.6, 46.1, 33.6, 26.1, 23.8, 23.4; HRMS [$M + H$]⁺: 561.2972; (calculated for $[C_{34}H_{36}N_6O_2]^+$: 561.2973).

Bis[(3-[(1,2,3,4-tetrahydroacridin-9-yl)amino]propyl)amino]cyclobut-3-ene-1,2-dione (**3b**). Yield 19%; yellow solid; M_p = 196–198 °C; ¹H-NMR (500 MHz, $DMSO-d_6$): δ 8.20–8.10 (m, 2H), 7.74–7.66 (m, 2H), 7.60–7.50 (m, 2H), 7.39–7.30 (m, 2H), 3.65–3.44 (m, 8H), 2.92–2.85 (m, 4H), 2.72–2.62 (m, 4H), 1.90–1.56 (m, 12H);

^{13}C -NMR (126 MHz, DMSO- d_6): δ 182.5, 159.2, 151.6, 147.3, 132.8, 126.5, 125.5, 123.7, 118.5, 116.1, 48.8, 44.9, 41.1, 33.5, 32.3, 25.2, 22.7, 22.3; HRMS $[\text{M} + \text{H}]^+$: 589.3218 (calculated for $[\text{C}_{36}\text{H}_{40}\text{N}_6\text{O}_2]^+$: 589.3286).

Bis({4-[(1,2,3,4-tetrahydroacridin-9-yl)amino]butyl}amino)cyclobut-3-ene-1,2-dione (**3c**). Yield 21%; yellow solid; Mp = 47–49 °C; ^1H -NMR (500 MHz, CD_3OD): δ 8.11–8.06 (m, 2H), 7.76–7.71 (m, 2H), 7.57–7.51 (m, 2H), 7.38–7.33 (m, 2H), 3.61–3.55 (m, 4H), 2.98–2.92 (m, 4H), 2.74–2.67 (m, 4H), 1.87 (dd, J = 7.3, 4.4 Hz, 8H), 1.69–1.63 (m, 8H), 1.31–1.24 (m, 4H); ^{13}C -NMR (126 MHz, CD_3OD): δ 183.5, 169.3, 158.5, 153.4, 147.0, 130.2, 127.2, 125.0, 124.5, 120.9, 116.7, 79.5, 60.2, 44.8, 33.7, 29.7, 28.9, 26.1, 23.9, 23.5, 8.5; HRMS $[\text{M} + \text{H}]^+$: 617.3603 (calculated for $[\text{C}_{38}\text{H}_{44}\text{N}_6\text{O}_2]^+$: 617.3599).

Bis({5-[(1,2,3,4-tetrahydroacridin-9-yl)amino]pentyl}amino)cyclobut-3-ene-1,2-dione (**3d**). Yield 15%; brown solid; Mp = 76–77 °C; ^1H -NMR (500 MHz, CDCl_3): δ 7.98–7.92 (m, 2H), 7.86–7.81 (m, 2H), 7.54–7.47 (m, 2H), 7.34–7.28 (m, 2H), 4.44–4.37 (m, 2H), 3.81 (bs, 5H), 3.63 (t, J = 7.0 Hz, 4H), 3.45 (q, J = 6.8 Hz, 4H), 3.03–2.96 (m, 4H), 2.66–2.60 (m, 4H), 1.89–1.83 (m, 8H), 1.67–1.60 (m, 8H), 1.47–1.36 (m, 4H); ^{13}C -NMR (126 MHz, CDCl_3): δ 182.2, 168.1, 157.3, 151.3, 146.1, 128.7, 126.9, 123.6, 123.0, 119.5, 115.2, 50.0, 48.8, 43.9, 32.9, 30.8, 30.6, 24.5, 23.5, 22.7, 22.3; HRMS $[\text{M} + \text{H}]^+$: 645.3903 (calculated for $[\text{C}_{40}\text{H}_{48}\text{N}_6\text{O}_2]^+$: 645.3912).

Bis({6-[(1,2,3,4-tetrahydroacridin-9-yl)amino]hexyl}amino)cyclobut-3-ene-1,2-dione (**3e**). Yield 56%; yellow solid; Mp = 93–95 °C; ^1H -NMR (500 MHz, CDCl_3): δ 7.90 (dd, J = 8.6, 1.4 Hz, 2H), 7.81 (dd, J = 8.5, 1.2 Hz, 2H), 7.66 (bs, 2H), 7.51–7.44 (m, 2H), 7.32–7.25 (m, 2H), 4.14 (t, J = 6.0 Hz, 2H), 3.62–3.53 (m, 4H), 3.39 (q, J = 6.7 Hz, 4H), 3.10 (bs, 2H), 3.02–2.91 (m, 4H), 2.67–2.55 (m, 4H), 1.91–1.78 (m, 8H), 1.60–1.46 (m, 8H), 1.34–1.19 (m, 8H); ^{13}C -NMR (126 MHz, CDCl_3): δ 182.4, 168.1, 157.9, 151.1, 146.9, 128.5, 127.8, 123.6, 122.9, 119.8, 115.5, 50.4, 49.0, 44.1, 33.6, 31.4, 30.9, 26.3, 25.9, 24.7, 22.9, 22.6; HRMS $[\text{M} + \text{H}]^+$: 673.4218 (calculated for $[\text{C}_{42}\text{H}_{52}\text{N}_6\text{O}_2]^+$: 673.4225).

Bis({7-[(1,2,3,4-tetrahydroacridin-9-yl)amino]heptyl}amino)cyclobut-3-ene-1,2-dione (**3f**). Yield 18%; yellow solid; Mp = 64–66 °C; ^1H -NMR (500 MHz, CD_3OD): δ 8.11 (d, J = 8.6 Hz, 2H), 7.75–7.70 (m, 2H), 7.61–7.55 (m, 2H), 7.40–7.34 (m, 2H), 3.61–3.53 (m, 8H), 3.00–2.92 (m, 4H), 2.72–2.66 (m, 4H), 1.94–1.84 (m, 8H), 1.68–1.61 (m, 4H), 1.58–1.51 (m, 4H), 1.38–1.29 (m, 12H); ^{13}C -NMR (126 MHz, CD_3OD): δ 183.5, 169.4, 157.4, 154.2, 146.1, 130.7, 126.2, 125.0, 124.9, 120.3, 115.8, 45.1, 33.1, 32.1, 32.0, 29.8, 27.7, 27.2, 25.9, 23.8, 23.3; HRMS $[\text{M} + \text{H}]^+$: 701.4534 (calculated for $[\text{C}_{44}\text{H}_{56}\text{N}_6\text{O}_2]^+$: 701.4538).

Bis({8-[(1,2,3,4-tetrahydroacridin-9-yl)amino]octyl}amino)cyclobut-3-ene-1,2-dione (**3g**). Yield 8%; yellow solid; Mp = 64–65 °C; ^1H -NMR (500 MHz, CDCl_3): δ 7.97 (d, J = 8.5 Hz, 2H), 7.91–7.78 (m, 4H), 7.51 (t, J = 7.6 Hz, 2H), 7.32 (t, J = 7.6 Hz, 2H), 4.34 (t, J = 6.0 Hz, 2H), 3.73–3.35 (m, 12H), 3.03–2.95 (m, 4H), 2.72–2.61 (m, 4H), 1.96–1.78 (m, 8H), 1.63–1.47 (m, 8H), 1.35–1.09 (m, 12H); ^{13}C -NMR (126 MHz, CDCl_3): δ 182.4, 168.2, 157.5, 151.6, 146.5, 128.8, 127.3, 123.7, 123.2, 119.6, 115.2, 50.4, 48.9, 44.3, 33.3, 31.5, 30.9, 28.8, 26.4, 26.1, 24.6, 22.8, 22.5; HRMS $[\text{M} + \text{H}]^+$: 729.4848 (calculated for $[\text{C}_{46}\text{H}_{60}\text{N}_6\text{O}_2]^+$: 729.4851).

Bis({2-[(6-chloro-1,2,3,4-tetrahydroacridin-9-yl)amino]ethyl}amino)cyclobut-3-ene-1,2-dione (**4a**). Yield 6%; yellow solid; Mp = 113–114 °C; ^1H -NMR (500 MHz, DMSO- d_6): δ 8.10 (d, J = 9.1 Hz, 2H), 7.72–7.66 (m, 2H), 7.35–7.24 (m, 2H), 3.73–3.43 (m, 8H), 2.91–2.75 (m, 4H), 2.70–2.59 (m, 4H), 1.80–1.67 (m, 8H); ^{13}C -NMR (126 MHz, DMSO- d_6): δ 182.6, 159.4, 150.5, 147.4, 132.7, 126.6, 125.5, 123.8, 118.8, 116.8, 69.9, 48.8, 44.3, 33.5, 25.1, 22.7, 22.3; HRMS $[\text{M} + \text{H}]^+$: 629.2179 (calculated for $[\text{C}_{34}\text{H}_{34}\text{Cl}_2\text{N}_6\text{O}_2]^+$: 629.2194).

Bis({3-[(6-chloro-1,2,3,4-tetrahydroacridin-9-yl)amino]propyl}amino)cyclobut-3-ene-1,2-dione (**4b**). Yield 28%; Mp = 86–88 °C; ^1H -NMR (500 MHz, DMSO- d_6): δ 8.11 (d, J = 9.1 Hz, 2H), 7.70–7.65 (m, 2H), 7.42 (bs, 2H), 7.32–7.25 (m, 2H), 3.52 (bs, 4H), 3.49–3.41 (m, 8H), 2.90–2.81 (m, 4H), 2.70–2.60 (m, 4H),

1.86–1.69 (m, 12H); ^{13}C -NMR (126 MHz, DMSO- d_6): δ 182.5, 159.2, 150.6, 147.3, 132.8, 126.5, 125.5, 123.67, 118.5, 116.1, 48.8, 44.9, 41.1, 33.5, 32.3, 25.2, 22.7, 22.3; HRMS $[\text{M} + \text{H}]^+$: 657.2513 (calculated for $[\text{C}_{36}\text{H}_{38}\text{Cl}_2\text{N}_6\text{O}_2]^+$: 657.2507).

Bis({4-[(6-chloro-1,2,3,4-tetrahydroacridin-9-yl)amino]butyl}amino)cyclobut-3-ene-1,2-dione (**4c**). Yield 59%; yellow solid; Mp = 99–100 °C; ^1H -NMR (500 MHz, DMSO- d_6): δ 8.13 (d, J = 9.1 Hz, 2H), 7.69 (d, J = 2.2 Hz, 2H), 7.42 (bs, 2H), 7.32 (dd, J = 9.0, 2.3 Hz, 2H), 3.64–3.27 (m, 8H), 2.90–2.82 (m, 4H), 2.68–2.60 (m, 4H), 1.84–1.66 (m, 8H), 1.60–1.46 (m, 8H); ^{13}C -NMR (126 MHz, DMSO- d_6): δ 182.4, 167.9, 158.8, 150.9, 146.9, 133.0, 126.1, 125.7, 123.8, 118.4, 115.9, 47.6, 43.1, 33.2, 28.3, 27.6, 25.1, 22.6, 22.2; HRMS $[\text{M} + \text{H}]^+$: 685.2819 (calculated for $[\text{C}_{38}\text{H}_{42}\text{Cl}_2\text{N}_6\text{O}_2]^+$: 685.2820).

Bis({5-[(6-chloro-1,2,3,4-tetrahydroacridin-9-yl)amino]pentyl}amino)cyclobut-3-ene-1,2-dione (**4d**). Yield 10%; yellow solid; Mp = 85–86 °C; ^1H -NMR (500 MHz, DMSO- d_6): δ 8.11 (d, J = 9.1 Hz, 2H), 7.69 (d, J = 2.3 Hz, 2H), 7.31 (dd, J = 9.1, 2.3 Hz, 2H), 3.42–3.24 (m, 8H), 2.92–2.81 (m, 4H), 2.71–2.60 (m, 4H), 1.84–1.69 (m, 8H), 1.62–1.52 (m, 4H), 1.51–1.40 (m, 4H), 1.35–1.23 (m, 4H); ^{13}C -NMR (126 MHz, DMSO- d_6): δ 182.4, 167.9, 159.4, 150.7, 147.6, 132.6, 126.7, 125.6, 123.6, 118.7, 116.1, 47.9, 43.3, 33.6, 30.6, 30.3, 25.2, 23.4, 22.7, 22.4; HRMS $[\text{M} + \text{H}]^+$: 713.3129 (calculated for $[\text{C}_{40}\text{H}_{46}\text{Cl}_2\text{N}_6\text{O}_2]^+$: 713.3133).

Bis({6-[(6-chloro-1,2,3,4-tetrahydroacridin-9-yl)amino]hexyl}amino)cyclobut-3-ene-1,2-dione (**4e**). Yield 36%; yellow solid; Mp = 87–88 °C; ^1H -NMR (500 MHz, DMSO- d_6): δ 8.11 (d, J = 9.1 Hz, 2H), 7.69 (d, J = 2.3 Hz, 2H), 7.31 (dd, J = 9.1, 2.3 Hz, 2H), 5.55 (t, J = 6.3 Hz, 2H), 4.10 (bs, 2H), 3.44–3.35 (m, 8H), 2.86 (t, J = 6.2 Hz, 4H), 2.65 (t, J = 6.0 Hz, 4H), 1.83–1.71 (m, 8H), 1.57–1.49 (m, 4H), 1.48–1.40 (m, 4H), 1.31–1.20 (m, 8H); ^{13}C -NMR (126 MHz, DMSO- d_6): δ 182.4, 167.9, 159.3, 150.7, 147.5, 132.7, 126.7, 125.6, 123.6, 118.7, 115.9, 48.0, 43.3, 33.6, 30.9, 30.6, 26.1, 25.7, 25.2, 22.7, 22.4; HRMS $[\text{M} + \text{H}]^+$: 741.3434 (calculated for $[\text{C}_{42}\text{H}_{50}\text{Cl}_2\text{N}_6\text{O}_2]^+$: 741.3446).

Bis({7-[(6-chloro-1,2,3,4-tetrahydroacridin-9-yl)amino]heptyl}amino)cyclobut-3-ene-1,2-dione (**4f**). Yield 87%; yellow solid; Mp = 85–86 °C; ^1H -NMR (500 MHz, CDCl_3): δ 7.85 (d, J = 9.1 Hz, 2H), 7.79 (d, J = 2.2 Hz, 2H), 7.54 (bs, 2H), 7.21 (dd, J = 9.0, 2.2 Hz, 2H), 4.12 (t, J = 6.0 Hz, 2H), 3.59 (q, J = 6.7 Hz, 4H), 3.43 (q, J = 6.7 Hz, 4H), 3.01–2.90 (m, 4H), 2.66–2.55 (m, 4H), 1.92–1.81 (m, 8H), 1.61–1.43 (m, 8H), 1.31–1.16 (m, 12H); ^{13}C -NMR (126 MHz, CDCl_3): δ 182.4, 168.1, 159.3, 151.1, 147.7, 134.1, 126.9, 124.8, 124.1, 118.2, 115.5, 50.6, 49.0, 44.4, 33.8, 31.4, 30.9, 28.6, 26.4, 26.2, 24.5, 22.8, 22.5; HRMS $[\text{M} + \text{H}]^+$: 769.3745 (calculated for $[\text{C}_{44}\text{H}_{54}\text{Cl}_2\text{N}_6\text{O}_2]^+$: 769.8446).

Bis({8-[(6-chloro-1,2,3,4-tetrahydroacridin-9-yl)amino]octyl}amino)cyclobut-3-ene-1,2-dione (**4g**). Yield 55%; brown solid; Mp = 58–60 °C; ^1H -NMR (500 MHz, CDCl_3): δ 7.87 (d, J = 9.0 Hz, 2H), 7.80 (d, J = 2.1 Hz, 2H), 7.60 (bs, 2H), 7.23 (dd, J = 9.0, 2.2 Hz, 2H), 4.13 (t, J = 6.0 Hz, 2H), 3.62 (q, J = 6.7 Hz, 4H), 3.47 (q, J = 6.7 Hz, 4H), 3.01–2.92 (m, 4H), 2.67–2.59 (m, 4H), 1.93–1.83 (m, 8H), 1.59 (p, J = 7.1 Hz, 4H), 1.51 (p, J = 7.0 Hz, 4H), 1.29–1.09 (m, 16H); ^{13}C -NMR (126 MHz, CDCl_3): δ 190.0, 189.8, 184.6, 184.4, 178.0, 177.4, 174.8, 174.7, 160.2, 160.2, 153.3, 148.5, 135.5, 126.6, 126.6, 126.5, 124.9, 119.4, 116.7, 70.6, 45.5, 45.3, 34.2, 32.2, 32.2, 31.8, 31.5, 30.2, 30.1, 30.1, 29.9, 27.8, 27.7, 27.3, 27.2, 25.9, 25.9, 23.9, 23.6, 16.2, 16.1; HRMS $[\text{M} + \text{H}]^+$: 797.4061 (calculated for $[\text{C}_{44}\text{H}_{54}\text{Cl}_2\text{N}_6\text{O}_2]^+$: 797.4072).

Bis({2-[(7-methoxy-1,2,3,4-tetrahydroacridin-9-yl)amino]ethyl}amino)cyclobut-3-ene-1,2-dione (**5a**). Yield 26%; yellow solid; Mp = 106–107 °C; ^1H -NMR (500 MHz, DMSO- d_6): δ 7.63 (d, J = 9.1 Hz, 2H), 7.51 (bs, 2H), 7.41–7.35 (m, 2H), 7.18 (dd, J = 9.1, 2.7 Hz, 2H), 5.36 (bs, 2H), 3.84 (s, 6H), 3.74–3.57 (m, 4H), 3.54–3.40 (m, 4H), 2.90–2.80 (m, 4H), 2.77–2.66 (m, 4H), 1.86–1.64 (m, 8H); ^{13}C -NMR (126 MHz, DMSO- d_6): δ 182.6, 168.1, 155.8, 155.6, 149.3, 142.4, 129.7, 121.5, 120.3, 117.9, 101.6, 55.5, 48.8, 48.4, 44.2, 33.2, 25.4, 22.9, 22.6; HRMS $[\text{M} + \text{H}]^+$: 621.3178 (calculated for $[\text{C}_{36}\text{H}_{40}\text{N}_6\text{O}_4]^+$: 621.3184).

Bis({3-[(7-methoxy-1,2,3,4-tetrahydroacridin-9-yl)amino]propyl}amino)cyclobut-3-ene-1,2-dione (**5b**). Yield 15%; yellow solid; Mp = 64–65 °C; ¹H-NMR (500 MHz, DMSO-*d*₆): δ 7.63 (d, *J* = 9.1 Hz, 2H), 7.42 (d, *J* = 2.6 Hz, 2H), 7.19 (dd, *J* = 9.1, 2.6 Hz, 2H), 5.48 (bs, 2H), 3.85 (s, 6H), 3.55 (bs, 4H), 3.42–3.31 (m, 8H), 2.86 (t, *J* = 6.5 Hz, 4H), 2.70 (t, *J* = 6.3 Hz, 4H), 1.85–1.69 (m, 12H); ¹³C-NMR (126 MHz, DMSO-*d*₆): δ 182.5, 167.9, 155.8, 155.5, 149.6, 142.3, 130.2, 129.6, 123.6, 121.3, 120.3, 118.8, 117.2, 101.6, 55.6, 44.5, 41.2, 33.1, 32.4, 25.6, 22.9, 22.6; HRMS [M + H]⁺: 649.3488 (calculated for [C₃₈H₄₄N₆O₄]⁺: 649.3497).

Bis({4-[(7-methoxy-1,2,3,4-tetrahydroacridin-9-yl)amino]butyl}amino)cyclobut-3-ene-1,2-dione (**5c**). Yield 61%; yellow solid; Mp = 91–92 °C; ¹H-NMR (500 MHz, CDCl₃): δ 7.84 (bs, 2H), 7.71 (d, *J* = 9.1 Hz, 2H), 7.18 (d, *J* = 2.7 Hz, 2H), 7.15 (d, *J* = 2.6 Hz, 1H), 7.14 (d, *J* = 2.6 Hz, 1H), 4.23–4.12 (m, 2H), 3.81 (s, 6H), 3.59–3.54 (m, 4H), 3.40–3.23 (m, 4H), 2.96–2.88 (m, 4H), 2.65–2.55 (m, 4H), 1.86–1.73 (m, 8H), 1.69–1.55 (m, 8H); ¹³C-NMR (126 MHz, CD₃OD): δ 183.5, 169.3, 157.7, 156.4, 152.4, 142.8, 128.9, 122.2, 118.0, 102.7, 56.1, 44.9, 33.6, 29.8, 28.9, 26.3, 24.0, 23.6; HRMS [M + H]⁺: 677.3799 (calculated for [C₄₀H₄₈N₆O₄]⁺: 677.3810).

Bis({5-[(7-methoxy-1,2,3,4-tetrahydroacridin-9-yl)amino]pentyl}amino)cyclobut-3-ene-1,2-dione (**5d**). Yield 50%; yellow solid; Mp = 70–72 °C; ¹H-NMR (500 MHz, CDCl₃): δ 7.85 (s, 2H), 7.73 (d, *J* = 9.1 Hz, 2H), 7.21 (d, *J* = 2.7 Hz, 2H), 7.17 (dd, *J* = 9.1, 2.6 Hz, 2H), 4.29–4.13 (m, 2H), 3.84 (s, 6H), 3.64–3.59 (m, 4H), 3.35 (q, *J* = 6.8 Hz, 4H), 2.94 (m, *J* = 6.8 Hz, 4H), 2.66–2.61 (m, 4H), 1.85–1.81 (m, 8H), 1.62–1.56 (m, 8H), 1.44–1.35 (m, 4H); ¹³C-NMR (126 MHz, CDCl₃): δ 182.4, 168.2, 156.0, 155.3, 150.6, 141.8, 128.5, 120.8, 120.8, 116.6, 101.9, 55.6, 48.4, 44.0, 32.9, 31.0, 30.7, 24.7, 23.7, 22.8, 22.5; HRMS [M + H]⁺: 705.4119 (calculated for [C₄₂H₅₂N₆O₄]⁺: 705.4123).

Bis({6-[(7-methoxy-1,2,3,4-tetrahydroacridin-9-yl)amino]hexyl}amino)cyclobut-3-ene-1,2-dione (**5e**). Yield 18%; yellow solid; Mp = 157–159 °C; ¹H-NMR (500 MHz, CDCl₃): δ 8.20 (bs, 2H), 7.75 (d, *J* = 9.2 Hz, 2H), 7.32 (d, *J* = 2.7 Hz, 2H), 7.18 (dd, *J* = 9.2, 2.6 Hz, 2H), 4.83 (bs, 2H), 4.20–3.93 (m, 4H), 3.87 (s, 6H), 3.67–3.60 (m, 4H), 2.99–2.94 (m, 4H), 2.70–2.65 (m, 4H), 1.88–1.81 (m, 8H), 1.69–1.55 (m, 10H), 1.47–1.32 (m, 10H); ¹³C-NMR (126 MHz, CDCl₃): δ 182.2, 168.3, 156.2, 154.1, 151.5, 140.2, 127.1, 121.4, 120.1, 115.4, 102.1, 55.7, 50.5, 48.1, 44.0, 32.0, 31.1, 30.7, 26.1, 25.8, 24.8, 22.7, 22.1; HRMS [M + H]⁺: 733.4434 (calculated for [C₄₄H₅₆N₆O₄]⁺: 733.4436).

Bis({7-[(7-methoxy-1,2,3,4-tetrahydroacridin-9-yl)amino]heptyl}amino)cyclobut-3-ene-1,2-dione (**5f**). Yield 16%; yellow solid; Mp = 132–134 °C; ¹H-NMR (500 MHz, CDCl₃): δ 8.32 (bs, 2H), 7.81 (dd, *J* = 9.5, 4.7 Hz, 2H), 7.36 (d, *J* = 2.6 Hz, 2H), 7.26–7.17 (m, 2H), 3.88 (s, 4H), 3.68–3.58 (m, 4H), 3.58–3.48 (m, 4H), 3.05–2.95 (m, 4H), 2.75–2.62 (m, 4H), 1.92–1.80 (m, 8H), 1.72–1.50 (m, 8H), 1.38–1.29 (m, 12H); ¹³C-NMR (126 MHz, CDCl₃): δ 182.2, 168.3, 156.2, 153.5, 152.0, 139.5, 126.5, 121.7, 119.8, 114.9, 102.4, 55.7, 53.4, 48.2, 44.2, 31.6, 31.1, 30.7, 28.5, 26.4, 25.9, 24.7, 22.7, 21.9; HRMS [M + H]⁺: 761.4736 (calculated for [C₄₆H₆₀N₆O₄]⁺: 761.4749).

Bis({8-[(7-methoxy-1,2,3,4-tetrahydroacridin-9-yl)amino]octyl}amino)cyclobut-3-ene-1,2-dione (**5g**). Yield 37%; yellow solid; Mp = 87–89 °C; ¹H-NMR (500 MHz, CDCl₃): δ 7.78–7.72 (m, 2H), 7.65 (bs, 2H), 7.25–7.19 (m, 4H), 3.95 (t, *J* = 6.4 Hz, 2H), 3.88 (s, 6H), 3.61 (q, *J* = 6.5 Hz, 4H), 3.43 (q, *J* = 6.7 Hz, 4H), 3.03–2.91 (m, 4H), 2.73–2.67 (m, 4H), 2.61 (bs, 2H), 1.93–1.83 (m, 8H), 1.58 (p, *J* = 7.0 Hz, 4H), 1.47 (m, 4H), 1.27–1.06 (m, 16H); ¹³C-NMR (126 MHz, CDCl₃): δ 182.6, 168.2, 155.9, 155.9, 150.6, 142.9, 129.3, 120.9, 120.6, 116.8, 101.9, 55.5, 50.5, 48.4, 44.3, 33.5, 31.8, 30.7, 28.8, 28.8, 26.4, 25.9, 24.7, 22.9, 22.7; HRMS [M + H]⁺: 789.5064 (calculated for [C₄₈H₆₄N₆O₄]⁺: 789.5062).

4.2. In Vitro Anti-ChE Assay

The AChE/BChE inhibitory activity of the tested drugs was determined using Ellman's method [47–50] and is expressed as IC₅₀, the i.e., concentration that reduces the cholinesterase activity by 50%. Human plasmatic butyrylcholinesterase (BChE; EC 3.1.1.8) and recombinant acetylcholinesterase

(AChE; 3.1.1.7) were prepared at the Department of Toxicology and Military Pharmacy. 5,5'-dithiobis (2-nitrobenzoic acid) (Ellman's reagent, DTNB), phosphate buffer (PB, pH 7.4), acetylthiocholine (ATC) and butyrylthiocholine (BTC), were purchased from Sigma-Aldrich, Prague, Czech Republic. For measuring purposes – polystyrene Nunc 96-well microplates with flat bottom shape (ThermoFisher Scientific, USA) were utilized.

All the assays were carried out in 0.1 M $\text{KH}_2\text{PO}_4/\text{K}_2\text{HPO}_4$ buffer, pH 7.4. Enzyme solutions were prepared at 2.0 units/mL in 2 mL aliquots. The assay medium (100 μL) consisted of 40 μL of 0.1 M phosphate buffer (pH 7.4), 20 μL of 0.01 M DTNB, 10 μL of the enzyme, and 20 μL of 0.01 M substrate (ATC/BTC iodide solution).

Inhibitor solutions in concentration range 10^{-3} – 10^{-11} M were prepared and IC_{50} values were calculated. Tested compounds were preincubated for 5 min. The reaction was started by immediate addition of 20 μL of the substrate. The activity was determined by measuring the increase in absorbance at 412 for AChE/BChE at 37 °C at 2 min intervals - using a Multi-mode microplate reader Synergy 2 (Winooski, VT, USA). Each concentration was assayed in triplicate. Software GraphPad Prism 5 (San Diego, CA, USA) was used for the statistical data evaluation.

4.3. Kinetic Study of AChE and BChE Inhibition

The kinetic study of AChE and BChE was performed by using the above-mentioned modified Ellman's method. The values of V_{max} and K_m of the Michaelis-Menten kinetics as well as the values of K_i and K_i' were calculated by nonlinear regression from the substrate velocity curves. Linear regression was used for calculation of Lineweaver-Burk plots. All calculations were performed using GraphPad Prism software version 6.07 for Windows (San Diego, CA, USA).

4.4. Evaluation of Cytotoxicity by MTT Assay

The human origin cell line HepG2 (ATCC, Manassas, VA, USA) isolated from liver hepatocellular carcinoma was used to evaluate cytotoxicity of tested compounds. The cells were cultivated in Dublecco's modified Eagle's medium (DMEM; Biosera, Nuaille, France) supplemented with 10% fetal bovine serum (Biosera) and 1% penicillin-streptomycin antibiotic solution (Sigma-Aldrich, St. Louis, MO, USA), incubated at 37 °C in a CO_2 incubator (Binder CO_2 incubator BC 160, Tuttlingen, Germany) and routinely passaged by trypsinization at 75–85% confluence.

The MTT (3-(4,5-dimethylthiazol-2-yl)-2,5-diphenyl-tetrazolium bromide (Sigma-Aldrich) reduction assay was used for measurement of compounds' cytotoxicity according to [68]. MTT is a water soluble tetrazolium salt and it is converted to purple formazan by succinate dehydrogenase in mitochondria of viable cells [69,70]. Cell viability was detected after 24-h incubation with the tested substances. For the assay, HepG2 cells were seeded into 96-well plates in 100 μL volume and density of 15×10^3 per well. Cells were allowed to attach overnight before the treatment. The stock solutions of tested compounds were prepared in dimethyl sulfoxide (DMSO; Sigma-Aldrich), which were further serially diluted in DMEM and added to the cells in 96-well culture plates. The final concentration of DMSO was less than 0.25% per well.

After 24-h incubation, the medium containing serially diluted substances was aspirated from each well and replaced by 100 μL of fresh medium containing MTT (0.5 mg/mL). Plates were subsequently incubated at 37 °C in CO_2 incubator for 45 min. The medium containing MTT was then aspirated and formazan dissolved in 100 μL of DMSO. The optical density of each well was measured using Synergy 2 Multi-Mode Microplate Reader (BioTek Instruments, Inc., Winooski, VT, USA) at 570 nm. The cell viability was expressed as the percentage of untreated control. Each experiment was performed in triplicate and repeated three independent times.

The IC_{50} values were calculated using four parametric nonlinear regression by statistic GraphPad Prism software (version 5.04; GraphPad Software Inc., San Diego, CA) from the logarithmic dose-response curve. The IC_{50} values were expressed as a mean \pm standard error of the mean (SEM).

4.5. Determination of *in Vitro* BBB Permeation

PAMPA (the parallel artificial membrane permeability assay) is a high-throughput screening tool applicable for prediction of the passive transport of potential drugs across the blood-brain barrier (BBB) [57]. In this study, it has been used as a non-cell-based *in vitro* assay carried out in a coated 96-well membrane filter. The filter membrane of the donor plate was coated with PBL (Polar Brain Lipid, Avanti, USA) in dodecane (4 μ l of 20 mg/mL PBL in dodecane) and the acceptor well was filled with 300 μ l of phosphate buffer saline, (PBS pH 7.4; V_A). The tested compounds were dissolved first in DMSO and then diluted with PBS pH 7.4 to reach the final concentrations 50–500 μ M in the donor well. The final concentration of DMSO did not exceed 0.5% (*v/v*) in the donor solution; 300 μ l of the donor solution (V_D) was added to the donor wells and the donor filter plate was carefully put on the acceptor plate so that the coated membrane was “in touch” with both donor solution and acceptor buffer. In principle, test compound diffuse from the donor well through the polar brain lipid membrane (area = 0.28 cm²) to the acceptor well. The concentration of the tested compound in both donor and the acceptor wells were assessed after 3, 4, 5 and 6 h of incubation in quadruplicate using the UV plate reader Synergy HT (Biotek, USA) at the maximum absorption wavelength of each compound ($n = 3$). Besides that, the solution of theoretical compound concentration, simulating the equilibrium state, established if the membrane was ideally permeable was prepared and assessed as well. The concentration of the compounds in the donor and acceptor well and equilibrium concentration were calculated from the standard curve and expressed as the permeability (Pe) according the equation [57]

$$\log Pe = \log \left\{ C \times - \ln \left(1 - \frac{[drug]_{acceptor}}{[drug]_{equilibrium}} \right) \right\} \quad (1)$$

where $C = \left(\frac{V_D \times V_A}{(V_D + V_A) \times Area \times Time} \right)$.

4.6. Molecular Modeling Studies

From the online PDB database (www.pdb.org) models of *hAChE* (PDB ID: 4EY7, resolution: 2.35 Å) and *hBChE* (PDB ID: 4BDS, resolution: 2.10 Å) were downloaded and prepared for flexible molecular docking by MGL Tools utilities [59,60]. The preparation of these receptors involved removal of the surplus copies of the enzyme chains, non-bonded inhibitors, addition of polar hydrogens and merging of non-polar ones. Default Gasteiger charges were assigned to all atoms. Flexible parts of the enzymes were determined by a spherical selection of residues ($R = 11$ Å) approximately around the center of the active site. In the same points, the centers of the grid box of $33 \times 33 \times 33$ Å were positioned. The rotatable bonds in the flexible residues were detected automatically by AutoDock Tools 1.5.4 program. Given the limitation of the program used for flexible molecular docking, water molecules had to be removed from the system. The flexible receptor parts contained 40 residues for *hAChE* and 39 residues for *hBChE*. The following xyz coordinates of the grid box centers were applied: *hAChE* (10.698, −58.115, −23.192); *hBChE* (140.117, 122.247, 38.986). The studied ligands were firstly drawn in HyperChem 8.0, then manually protonated as suggested by MarvinSketch 6.2.0. software (<http://www.chemaxon.com>), geometrically optimized by semi-empirical quantum-chemistry PM3 method and stored as pdb files. The structures of the ligands were processed for docking in a similar way as abovementioned flexible parts of the receptor by AutoDock Tools 1.5.4 program. Molecular docking was carried out in AutoDock Vina 1.1.2 program utilizing computer resources of the Czech National Grid Infrastructure MetaCentrum. The search algorithm of AutoDock Vina efficiently combines a Markov chain Monte Carlo like method for the global search and a Broyden-Fletcher-Goldfarb-Shano gradient approach for the local search [61]. It is a type of memetic algorithm based on interleaving stochastic and deterministic calculations [70]. Each docking task was repeated 20 times with the exhaustiveness parameter set to 16, employing 16 CPUs in parallel multithreading. From the obtained results, the solutions reaching the minimum predicted Gibbs binding energy were taken as the top-scoring modes. The graphic

representations of the docked poses were shown in PyMOL (The PyMOL Molecular Graphics System, Version 1.5.0.4 Schrödinger, LLC). 2D diagrams were generated using Discovery Studio Visualizer v16.1.0.15350 (Dassault Systèmes Biovia Corp., 2016, San Diego, CA, USA).

Supplementary Materials: The data containing ^1H and ^{13}C NMR spectra are available online at <http://www.mdpi.com/2218-273X/9/8/379/s1>.

Author Contributions: Organic synthesis, writing original draft, NMR spectra interpretation, B.S. and E.M.; in vitro measurement of cholinesterase activity, V.H. and M.H.; cytotoxicity screening, L.M.; BBB permeation prediction, T.K. and O.S.; enzyme kinetic analysis, D.J.; NMR measurement, M.L.J.; in silico data interpretation, J.K.; supervision, J.K. and J.M.-C.

Funding: This project was conceived by JMC (IQOG, CSIC, Madrid, Spain), initially carried out experimentally by EM, in Madrid, thanks to a Short-Term Scientific Mission (from 30 January until the 28 April 2017) granted by EU COST Action (CA15135: “Multi-target paradigm for innovative ligand identification in the drug discovery process (MuTaLig)”), and continued in Hradec Kralove (Czech Republic) by EM in collaboration with BS, under the supervision of JK, who organized and planned all the biological analysis and wrote the manuscript. JMC is very thankful to EM, BS, and JK for their collaboration, and to the COST Action CA15135 for supporting this project. The study was supported by a grant of Ministry of Defence “Long Term Development Plan” Medical Aspects of Weapons of Mass Destruction of the Faculty of Military Health Sciences, University of Defence, by the Ministry of Education, Youth and Sports of Czech Republic (project ERDF no. CZ.02.1.01/0.0/0.0/18_069/0010054) and by MH CZ - DRO (University Hospital Hradec Kralove, No. 00179906). JMC thanks MINECO (Government of Spain) (SAF2015-65586-R) for support.

Acknowledgments: The authors express their appreciation to L. Krbalek for her excellent technical assistance.

Conflicts of Interest: The authors have declared no conflict of interest.

References

1. Ferri, C.P.; Prince, M.; Brayne, C.; Brodaty, H.; Fratiglioni, L.; Ganguli, M.; Hall, K.; Hasegawa, K.; Hendrie, H.; Huang, Y.; et al. Global prevalence of dementia: a Delphi consensus study. *Lancet* **2005**, *366*, 2112–2117. [[CrossRef](#)]
2. Long, J.Z.; Cravatt, B.F. The Metabolic Serine Hydrolases and Their Functions in Mammalian Physiology and Disease. *Chem. Rev.* **2011**, *111*, 6022–6063. [[CrossRef](#)] [[PubMed](#)]
3. Bartus, R.T.; Dean, R.L.; Beer, B.; Lippa, A.S. The cholinergic hypothesis of geriatric memory dysfunction. *Science* **1982**, *217*, 408–414. [[CrossRef](#)] [[PubMed](#)]
4. Zemek, F.; Drtinova, L.; Nepovimova, E.; Sepsova, V.; Korabecny, J.; Klimes, J.; Kuca, K. Outcomes of Alzheimer’s disease therapy with acetylcholinesterase inhibitors and memantine. *Expert Opin. Drug Saf.* **2014**, *13*, 759–774.
5. Birks, J. Cholinesterase inhibitors for Alzheimer’s disease. *Cochrane Database Syst. Rev.* **2006**, CD005593.
6. Vickers, J.C.; Mitew, S.; Woodhouse, A.; Fernandez-Martos, C.M.; Kirkcaldie, M.T.; Canty, A.J.; McCormack, G.H.; King, A.E. Defining the earliest pathological changes of Alzheimer’s disease. *Curr. Alzheimer Res.* **2016**, *13*, 281–287. [[CrossRef](#)] [[PubMed](#)]
7. Kim, G.H.; Kim, J.E.; Rhie, S.J.; Yoon, S. The Role of Oxidative Stress in Neurodegenerative Diseases. *Exp. Neurobiol.* **2015**, *24*, 325–340. [[CrossRef](#)]
8. Wang, R.; Reddy, P.H. Role of Glutamate and NMDA Receptors in Alzheimer’s Disease. *J. Alzheimers Dis. JAD* **2017**, *57*, 1041–1048. [[CrossRef](#)]
9. Budimir, A. Metal ions, Alzheimer’s disease and chelation therapy. *Acta Pharm. Zagreb Croat.* **2011**, *61*, 1–14. [[CrossRef](#)]
10. Heneka, M.T.; Carson, M.J.; El Khoury, J.; Landreth, G.E.; Brosseron, F.; Feinstein, D.L.; Jacobs, A.H.; Wyss-Coray, T.; Vitorica, J.; Ransohoff, R.M.; et al. Neuroinflammation in Alzheimer’s Disease. *Lancet Neurol.* **2015**, *14*, 388–405. [[CrossRef](#)]
11. Sonkusare, S.K.; Kaul, C.L.; Ramarao, P. Dementia of Alzheimer’s disease and other neurodegenerative disorders—memantine, a new hope. *Pharmacol. Res.* **2005**, *51*, 1–17. [[CrossRef](#)] [[PubMed](#)]
12. Crismon, M.L. Tacrine: first drug approved for Alzheimer’s disease. *Ann. Pharmacother.* **1994**, *28*, 744–751. [[CrossRef](#)] [[PubMed](#)]

13. Horak, M.; Holubova, K.; Nepovimova, E.; Krusek, J.; Kaniakova, M.; Korabecny, J.; Vyklicky, L.; Kuca, K.; Stuchlik, A.; Ricny, J.; et al. The pharmacology of tacrine at N-methyl-d-aspartate receptors. *Prog. Neuropsychopharmacol. Biol. Psychiatry* **2017**, *75*, 54–62. [CrossRef] [PubMed]
14. Soukup, O.; Jun, D.; Zdarova-Karasova, J.; Patocka, J.; Musilek, K.; Korabecny, J.; Krusek, J.; Kaniakova, M.; Sepsova, V.; Mandikova, J.; et al. A resurrection of 7-MEOTA: a comparison with tacrine. *Curr. Alzheimer Res.* **2013**, *10*, 893–906. [CrossRef] [PubMed]
15. Lahiri, D.K.; Lewis, S.; Farlow, M.R. Tacrine alters the secretion of the beta-amyloid precursor protein in cell lines. *J. Neurosci. Res.* **1994**, *37*, 777–787. [CrossRef] [PubMed]
16. Lahiri, D.K.; Farlow, M.R.; Sambamurti, K. The secretion of amyloid beta-peptides is inhibited in the tacrine-treated human neuroblastoma cells. *Brain Res. Mol. Brain Res.* **1998**, *62*, 131–140. [CrossRef]
17. Watkins, P.B.; Zimmerman, H.J.; Knapp, M.J.; Gracon, S.I.; Lewis, K.W. Hepatotoxic effects of tacrine administration in patients with Alzheimer's disease. *JAMA* **1994**, *271*, 992–998. [CrossRef]
18. Zeiger, E.; Erexson, G.; Mortelmans, K.; Thilagar, A. Genetic toxicity studies of 1,2,3,4-tetrahydro-9-acridinamine (tacrine). *Mutat. Res.* **1997**, *393*, 189–197. [CrossRef]
19. Misik, J.; Nepovimova, E.; Pejchal, J.; Kassa, J.; Korabecny, J.; Soukup, O. Cholinesterase Inhibitor 6-Chlorotacrine—In Vivo Toxicological Profile and Behavioural Effects. Available online: <http://www.eurekaselect.com/158225/article> (accessed on 2 August 2019).
20. Pang, Y.P.; Quiram, P.; Jelacic, T.; Hong, F.; Brimijoin, S. Highly potent, selective, and low cost bis-tetrahydroaminacrine inhibitors of acetylcholinesterase. Steps toward novel drugs for treating Alzheimer's disease. *J. Biol. Chem.* **1996**, *271*, 23646–23649. [CrossRef]
21. Recanatini, M.; Cavalli, A.; Belluti, F.; Piazzini, L.; Rampa, A.; Bisi, A.; Gobbi, S.; Valenti, P.; Andrisano, V.; Bartolini, M.; et al. SAR of 9-amino-1,2,3,4-tetrahydroacridine-based acetylcholinesterase inhibitors: synthesis, enzyme inhibitory activity, QSAR, and structure-based CoMFA of tacrine analogues. *J. Med. Chem.* **2000**, *43*, 2007–2018. [CrossRef]
22. Carlier, P.R.; Han, Y.F.; Chow, E.S.; Li, C.P.; Wang, H.; Lieu, T.X.; Wong, H.S.; Pang, Y.P. Evaluation of short-tether bis-THA AChE inhibitors. A further test of the dual binding site hypothesis. *Bioorg. Med. Chem.* **1999**, *7*, 351–357. [CrossRef]
23. Korábečný, J. Prokognitivní Potenciál Bis(7)-takrinu Jako Zvažovaného Terapeutika Neurodegenerativních Onemocnění. *MMSL* **2018**, *87*, 34–44. [CrossRef]
24. Chauhan, P.; Mahajan, S.; Kaya, U.; Hack, D.; Enders, D. Bifunctional Amine-Squaramides: Powerful Hydrogen-Bonding Organocatalysts for Asymmetric Domino/Cascade Reactions. *Adv. Synth. Catal.* **2015**, *357*, 253–281. [CrossRef]
25. Zhao, B.-L.; Li, J.-H.; Du, D.-M. Squaramide-Catalyzed Asymmetric Reactions. *Chem. Rec.* **2017**, *17*, 994–1018. [CrossRef]
26. Karahan, S.; Tanyeli, C. Squaramide catalyzed α -chiral amine synthesis. *Tetrahedron Lett.* **2018**, *59*, 3725–3737. [CrossRef]
27. Brandão, P.; Burke, A.J. Recent advances in the asymmetric catalytic synthesis of chiral 3-hydroxy and 3-aminoxindoles and derivatives: Medicinally relevant compounds. *Tetrahedron* **2018**, *74*, 4927–4957. [CrossRef]
28. Kinney, W.A.; Abou-Gharbia, M.; Garrison, D.T.; Schmid, J.; Kowal, D.M.; Bramlett, D.R.; Miller, T.L.; Tasse, R.P.; Zaleska, M.M.; Moyer, J.A. Design and Synthesis of [2-(8,9-Dioxo-2,6-diazabicyclo[5.2.0]non-1(7)-en-2-yl)-ethyl]phosphonic Acid (EAA-090), a Potent N-Methyl-d-aspartate Antagonist, via the Use of 3-Cyclobutene-1,2-dione as an Achiral α -Amino Acid Bioisostere. *J. Med. Chem.* **1998**, *41*, 236–246. [CrossRef]
29. Dwyer, M.P.; Yu, Y.; Chao, J.; Aki, C.; Chao, J.; Biju, P.; Girijavallabhan, V.; Rindgen, D.; Bond, R.; Mayer-Ezel, R.; et al. Discovery of 2-Hydroxy-N,N-dimethyl-3-{2-[[[(R)-1-(5-methylfuran-2-yl)propyl]amino]-3,4-dioxocyclobut-1-enylamino]benzamide (SCH 527123): A Potent, Orally Bioavailable CXCR2/CXCR1 Receptor Antagonist. *J. Med. Chem.* **2006**, *49*, 7603–7606. [CrossRef]
30. Storer, R.I.; Aciro, C.; Jones, L.H. Squaramides: physical properties, synthesis and applications. *Chem. Soc. Rev.* **2011**, *40*, 2330–2346. [CrossRef]
31. Marín, C.; Ximenis, M.; Ramirez-Macías, I.; Rotger, C.; Urbanova, K.; Olmo, F.; Martín-Escolano, R.; Rosales, M.J.; Cañas, R.; Gutierrez-Sánchez, R.; et al. Effective anti-leishmanial activity of minimalist squaramide-based compounds. *Exp. Parasitol.* **2016**, *170*, 36–49. [CrossRef]

32. Ribeiro, C.J.A.; Espadinha, M.; Machado, M.; Gut, J.; Gonçalves, L.M.; Rosenthal, P.J.; Prudêncio, M.; Moreira, R.; Santos, M.M.M. Novel squaramides with in vitro liver stage antiplasmodial activity. *Bioorg. Med. Chem.* **2016**, *24*, 1786–1792. [[CrossRef](#)]
33. Martín-Escolano, R.; Marín, C.; Vega, M.; Martín-Montes, Á.; Medina-Carmona, E.; López, C.; Rotger, C.; Costa, A.; Sánchez-Moreno, M. Synthesis and biological evaluation of new long-chain squaramides as anti-chagasic agents in the BALB/c mouse model. *Bioorg. Med. Chem.* **2019**, *27*, 865–879. [[CrossRef](#)]
34. Fu, H.; Li, W.; Luo, J.; Lee, N.T.K.; Li, M.; Tsim, K.W.K.; Pang, Y.; Youdim, M.B.H.; Han, Y. Promising anti-Alzheimer's dimer bis(7)-tacrine reduces β -amyloid generation by directly inhibiting BACE-1 activity. *Biochem. Biophys. Res. Commun.* **2008**, *366*, 631–636. [[CrossRef](#)]
35. Li, C.; Carlier, P.R.; Ren, H.; Kan, K.K.W.; Hui, K.; Wang, H.; Li, W.; Li, Z.; Xiong, K.; Clement, E.C.; et al. Alkylene tether-length dependent γ -aminobutyric acid type A receptor competitive antagonism by tacrine dimers. *Neuropharmacology* **2007**, *52*, 436–443. [[CrossRef](#)]
36. Ros, E.; Aleu, J.; Gomez De Aranda, I.; Cantí, C.; Pang, Y.-P.; Marsal, J.; Solsona, C. Effects of Bis(7)-Tacrine on Spontaneous Synaptic Activity and on the Nicotinic ACh Receptor of Torpedo Electric Organ. *J. Neurophysiol.* **2001**, *86*, 183–189. [[CrossRef](#)]
37. Minarini, A.; Milelli, A.; Tumiatti, V.; Rosini, M.; Simoni, E.; Bolognesi, M.L.; Andrisano, V.; Bartolini, M.; Motori, E.; Angeloni, C.; et al. Cystamine-tacrine dimer: A new multi-target-directed ligand as potential therapeutic agent for Alzheimer's disease treatment. *Neuropharmacology* **2012**, *62*, 997–1003. [[CrossRef](#)]
38. Han, Y.-F.; Wu, D.-C.; Xiao, X.-Q.; Chen, P.M.Y.; Chung, W.; Lee, N.T.K.; Pang, Y.-P.; Carlier, P.R. Protection against ischemic injury in primary cultured astrocytes of mouse cerebral cortex by bis(7)-tacrine, a novel anti-Alzheimer's agent. *Neurosci. Lett.* **2000**, *288*, 95–98. [[CrossRef](#)]
39. Zhao, Y.; Li, W.; Chow, P.C.Y.; Lau, D.T.K.; Lee, N.T.K.; Pang, Y.; Zhang, X.; Wang, X.; Han, Y. Bis(7)-tacrine, a promising anti-Alzheimer's dimer, affords dose- and time-dependent neuroprotection against transient focal cerebral ischemia. *Neurosci. Lett.* **2008**, *439*, 160–164. [[CrossRef](#)]
40. Li, J.; Lu, Z.; Xu, L.; Wang, Q.; Zhang, Z.; Fang, J. Neuroprotective effects of bis(7)-tacrine in a rat model of pressure-induced retinal ischemia. *Cell Biochem. Biophys.* **2014**, *68*, 275–282. [[CrossRef](#)]
41. Xiao, X.Q.; Lee, N.T.; Carlier, P.R.; Pang, Y.; Han, Y.F. Bis(7)-tacrine, a promising anti-Alzheimer's agent, reduces hydrogen peroxide-induced injury in rat pheochromocytoma cells: comparison with tacrine. *Neurosci. Lett.* **2000**, *290*, 197–200. [[CrossRef](#)]
42. Li, W.; Xue, J.; Niu, C.; Fu, H.; Lam, C.S.C.; Luo, J.; Chan, H.H.N.; Xue, H.; Kan, K.K.W.; Lee, N.T.K.; et al. Synergistic Neuroprotection by Bis(7)-tacrine via Concurrent Blockade of N-Methyl-d-aspartate Receptors and Neuronal Nitric-Oxide Synthase. *Mol. Pharmacol.* **2007**, *71*, 1258–1267. [[CrossRef](#)]
43. Li, W.; Lee, N.T.K.; Fu, H.; Kan, K.K.W.; Pang, Y.-P.; Li, M.; Tsim, K.W.K.; Li, X.; Han, Y. Neuroprotection via inhibition of nitric oxide synthase by bis(7)-tacrine. *NeuroReport* **2006**, *17*, 471–474. [[CrossRef](#)]
44. Li, W.; Pi, R.; Chan, H.H.N.; Fu, H.; Lee, N.T.K.; Tsang, H.W.; Pu, Y.; Chang, D.C.; Li, C.; Luo, J.; et al. Novel dimeric acetylcholinesterase inhibitor bis7-tacrine, but not donepezil, prevents glutamate-induced neuronal apoptosis by blocking N-methyl-D-aspartate receptors. *J. Biol. Chem.* **2005**, *280*, 18179–18188. [[CrossRef](#)]
45. Nepovimova, E.; Korabecny, J.; Dolezal, R.; Babkova, K.; Ondrejcek, A.; Jun, D.; Sepsova, V.; Horova, A.; Hrabanova, M.; Soukup, O.; et al. Tacrine-Trolox Hybrids: A Novel Class of Centrally Active, Nonhepatotoxic Multi-Target-Directed Ligands Exerting Anticholinesterase and Antioxidant Activities with Low In Vivo Toxicity. *J. Med. Chem.* **2015**, *58*, 8985–9003. [[CrossRef](#)]
46. Spilovska, K.; Korabecny, J.; Kral, J.; Horova, A.; Musilek, K.; Soukup, O.; Drtinova, L.; Gazova, Z.; Siposova, K.; Kuca, K. 7-Methoxytacrine-adamantylamine heterodimers as cholinesterase inhibitors in Alzheimer's disease treatment—synthesis, biological evaluation and molecular modeling studies. *Molecules* **2013**, *18*, 2397–2418. [[CrossRef](#)]
47. Ellman, G.L.; Courtney, K.D.; Andres, V.; Feather-Stone, R.M. A new and rapid colorimetric determination of acetylcholinesterase activity. *Biochem. Pharmacol.* **1961**, *7*, 88–95. [[CrossRef](#)]
48. Pohanka, M.; Jun, D.; Kuca, K. Improvement of acetylcholinesterase-based assay for organophosphates in way of identification by reactivators. *Talanta* **2008**, *77*, 451–454. [[CrossRef](#)]
49. Sepsova, V.; Karasova, J.Z.; Korabecny, J.; Dolezal, R.; Zemek, F.; Bennion, B.J.; Kuca, K. Oximes: inhibitors of human recombinant acetylcholinesterase. A structure-activity relationship (SAR) study. *Int. J. Mol. Sci.* **2013**, *14*, 16882–16900. [[CrossRef](#)]

50. Pohanka, M.; Karasova, J.Z.; Kuca, K.; Pikula, J.; Holas, O.; Korabecny, J.; Cabal, J. Colorimetric dipstick for assay of organophosphate pesticides and nerve agents represented by paraoxon, sarin and VX. *Talanta* **2010**, *81*, 621–624. [[CrossRef](#)]
51. Bolognesi, M.L.; Cavalli, A.; Valgimigli, L.; Bartolini, M.; Rosini, M.; Andrisano, V.; Recanatini, M.; Melchiorre, C. Multi-Target-Directed Drug Design Strategy: From a Dual Binding Site Acetylcholinesterase Inhibitor to a Trifunctional Compound against Alzheimer's Disease. *J. Med. Chem.* **2007**, *50*, 6446–6449. [[CrossRef](#)]
52. Nordberg, A.; Ballard, C.; Bullock, R.; Darreh-Shori, T.; Somogyi, M. A review of butyrylcholinesterase as a therapeutic target in the treatment of Alzheimer's disease. *Prim. Care Companion CNS Disord.* **2013**, *15*. [[CrossRef](#)]
53. Greig, N.H.; Utsuki, T.; Ingram, D.K.; Wang, Y.; Pepeu, G.; Scali, C.; Yu, Q.-S.; Mamczarz, J.; Holloway, H.W.; Giordano, T.; et al. Selective butyrylcholinesterase inhibition elevates brain acetylcholine, augments learning and lowers Alzheimer beta-amyloid peptide in rodent. *Proc. Natl. Acad. Sci. USA* **2005**, *102*, 17213–17218. [[CrossRef](#)]
54. Nepovimova, E.; Uliassi, E.; Korabecny, J.; Peña-Altamira, L.E.; Samez, S.; Pesaresi, A.; Garcia, G.E.; Bartolini, M.; Andrisano, V.; Bergamini, C.; et al. Multitarget drug design strategy: quinone-tacrine hybrids designed to block amyloid- β aggregation and to exert anticholinesterase and antioxidant effects. *J. Med. Chem.* **2014**, *57*, 8576–8589. [[CrossRef](#)]
55. Spilovska, K.; Korabecny, J.; Horova, A.; Musilek, K.; Nepovimova, E.; Drtinova, L.; Gazova, Z.; Siposova, K.; Dolezal, R.; Jun, D.; et al. Design, synthesis and in vitro testing of 7-methoxytacrine-amantadine analogues: a novel cholinesterase inhibitors for the treatment of Alzheimer's disease. *Med. Chem. Res.* **2015**, *24*, 2645–2655. [[CrossRef](#)]
56. Muckova, L.; Pejchal, J.; Jost, P.; Vanova, N.; Herman, D.; Jun, D. Cytotoxicity of acetylcholinesterase reactivators evaluated in vitro and its relation to their structure. *Drug Chem. Toxicol.* **2019**, *42*, 252–256. [[CrossRef](#)]
57. Di, L.; Kerns, E.H.; Fan, K.; McConnell, O.J.; Carter, G.T. High throughput artificial membrane permeability assay for blood-brain barrier. *Eur. J. Med. Chem.* **2003**, *38*, 223–232. [[CrossRef](#)]
58. Li, C.; Wainhaus, S.; Uss, A.S.; Cheng, K.-C. High-Throughput Screening Using Caco-2 Cell and PAMPA Systems. In *Drug Absorption Studies: In Situ, In Vitro and In Silico Models*; Ehrhardt, C., Kim, K.-J., Eds.; Biotechnology: Pharmaceutical Aspects; Springer US: Boston, MA, USA, 2008; pp. 418–429. ISBN 978-0-387-74901-3.
59. Cheung, J.; Rudolph, M.J.; Burshteyn, F.; Cassidy, M.S.; Gary, E.N.; Love, J.; Franklin, M.C.; Height, J.J. Structures of human acetylcholinesterase in complex with pharmacologically important ligands. *J. Med. Chem.* **2012**, *55*, 10282–10286. [[CrossRef](#)]
60. Nachon, F.; Carletti, E.; Ronco, C.; Trovaslet, M.; Nicolet, Y.; Jean, L.; Renard, P.-Y. Crystal structures of human cholinesterases in complex with huprine W and tacrine: elements of specificity for anti-Alzheimer's drugs targeting acetyl- and butyryl-cholinesterase. *Biochem. J.* **2013**, *453*, 393–399. [[CrossRef](#)]
61. Trott, O.; Olson, A.J. AutoDock Vina: Improving the speed and accuracy of docking with a new scoring function, efficient optimization and multithreading. *J. Comput. Chem.* **2010**, *31*, 455–461. [[CrossRef](#)]
62. Hepnarova, V.; Korabecny, J.; Matouskova, L.; Jost, P.; Muckova, L.; Hrabnova, M.; Vykoukalova, N.; Kerhartova, M.; Kucera, T.; Dolezal, R.; et al. The concept of hybrid molecules of tacrine and benzyl quinolone carboxylic acid (BQCA) as multifunctional agents for Alzheimer's disease. *Eur. J. Med. Chem.* **2018**, *150*, 292–306. [[CrossRef](#)]
63. Rydberg, E.H.; Brumshtein, B.; Greenblatt, H.M.; Wong, D.M.; Shaya, D.; Williams, L.D.; Carlier, P.R.; Pang, Y.-P.; Silman, I.; Sussman, J.L. Complexes of alkylene-linked tacrine dimers with *Torpedo californica* acetylcholinesterase: Binding of Bis5-tacrine produces a dramatic rearrangement in the active-site gorge. *J. Med. Chem.* **2006**, *49*, 5491–5500. [[CrossRef](#)]
64. Bajda, M.; Więckowska, A.; Hebda, M.; Guzior, N.; Sotriffer, C.A.; Malawska, B. Structure-Based Search for New Inhibitors of Cholinesterases. *Int. J. Mol. Sci.* **2013**, *14*, 5608–5632. [[CrossRef](#)]
65. Cavalli, A.; Bolognesi, M.L.; Minarini, A.; Rosini, M.; Tumiatti, V.; Recanatini, M.; Melchiorre, C. Multi-target-directed ligands to combat neurodegenerative diseases. *J. Med. Chem.* **2008**, *51*, 347–372. [[CrossRef](#)]

66. León, R.; Garcia, A.G.; Marco-Contelles, J. Recent advances in the multitarget-directed ligands approach for the treatment of Alzheimer's disease. *Med. Res. Rev.* **2013**, *33*, 139–189. [[CrossRef](#)]
67. Proschak, E.; Stark, H.; Merk, D. Polypharmacology by Design: A Medicinal Chemist's Perspective on Multitargeting Compounds. *J. Med. Chem.* **2019**, *62*, 420–444. [[CrossRef](#)]
68. Mosmann, T. Rapid colorimetric assay for cellular growth and survival: Application to proliferation and cytotoxicity assays. *J. Immunol. Methods* **1983**, *65*, 55–63. [[CrossRef](#)]
69. Riss, T.L.; Moravec, R.A.; Niles, A.L.; Duellman, S.; Benink, H.A.; Worzella, T.J.; Minor, L. Cell Viability Assays. In *Assay Guidance Manual*; Sittampalam, G.S., Coussens, N.P., Nelson, H., Arkin, M., Auld, D., Austin, C., Bejcek, B., Glicksman, M., Inglesse, J., Iversen, P.W., et al., Eds.; Eli Lilly & Company and the National Center for Advancing Translational Sciences: Bethesda, MD, USA, 2004.
70. Liu, B.; Wang, L.; Jin, Y.-H. An effective PSO-based memetic algorithm for flow shop scheduling. *IEEE Trans. Syst. Man Cybern. Part B Cybern. Publ. IEEE Syst. Man Cybern. Soc.* **2007**, *37*, 18–27. [[CrossRef](#)]



© 2019 by the authors. Licensee MDPI, Basel, Switzerland. This article is an open access article distributed under the terms and conditions of the Creative Commons Attribution (CC BY) license (<http://creativecommons.org/licenses/by/4.0/>).